This document is downloaded from DR-NTU (https://dr.ntu.edu.sg)
Nanyang Technological University, Singapore.

Southwest Pacific Ocean response to a warming world : using Mg/Ca, Zn/Ca, and Mn/Ca in foraminifera to track surface ocean water masses during the last deglaciation

Carter, Lionel; Bolton, Annette; Smith, Euan; Marr, Julene P.; Bostock, Helen C.

2013

Marr, J. P., Carter, L., Bostock, H. C., Bolton, A., & Smith, E. (2013). Southwest Pacific Ocean response to a warming world: Using Mg/Ca, Zn/Ca, and Mn/Ca in foraminifera to track surface ocean water masses during the last deglaciation. Paleoceanography, 28, 1–16.

https://hdl.handle.net/10356/80085

https://doi.org/10.1002/palo.20032

© 2013 American Geophysical Union. This paper was published in Paleoceanography and is made available as an electronic reprint (preprint) with permission of American Geophysical Union. The paper can be found at the following official DOI: [http://dx.doi.org/10.1002/palo.20032]. One print or electronic copy may be made for personal use only. Systematic or multiple reproduction, distribution to multiple locations via electronic or other means, duplication of any material in this paper for a fee or for commercial purposes, or modification of the content of the paper is prohibited and is subject to penalties under law.

Downloaded on 23 Aug 2022 16:02:40 SGT

PALEOCEANOGRAPHY, VOL. 28, 1–16, doi:10.1002/palo.20032, 2013

Southwest Pacific Ocean response to a warming world: Using Mg/Ca, Zn/Ca, and Mn/Ca in foraminifera to track surface ocean water masses during the last deglaciation

Julene P. Marr,[1,2] Lionel Carter,[2] Helen C. Bostock,[3] Annette Bolton,[4] and Euan Smith[1]

Received 13 June 2012; revised 3 April 2013; accepted 23 May 2013.

[1] In situ measurements of Mg/Ca, Zn/Ca, Mn/Ca, and Ba/Ca in *Globigerinoides bulloides* and *Globigerina ruber* from southwest Pacific core top sites and plankton tow are reported and their potential as paleoproxies is explored. The modern samples cover 20° of latitude from 34°S to 54°S, 7–19°C water temperature, and variable influence of subantarctic (SAW) and subtropical (STW) surface waters. Trace element signatures recorded in core top and plankton tow planktic foraminifera are examined in the context of the chemistry and nutrient profiles of their modern water masses. Our observations suggest that Zn/Ca and Mn/Ca may have the potential to trace SAW and STW. Intraspecies and interspecies offsets identified by in situ measurements of Mg/Ca and Zn/Ca indicate that these ratios may also record changes in thermal and nutrient stratification in the upper ocean. We apply these potential proxies to fossilized foraminifera from the high-resolution core MD97 2121. At the Last Glacial Maximum, surface water Mg/Ca temperature estimates indicate that temperatures were approximately 6–7°C lower than those of the present, accompanied by low levels of Mn/Ca and Zn/Ca and minimal thermal and nutrient stratification. This is consistent with regional dominance of SAW and reduced STW inflow associated with a reduced South Pacific Gyre (SPG). Upper ocean thermal and nutrient stratification collapsed during the Antarctic Cold Reversal, before poleward migration of the zonal winds and ocean fronts invigorated the SPG and increased STW inflow in the early Holocene. Together with reduced winds, this favored a stratified upper ocean from circa 10 ka to the present.

Citation: Marr, J. P., L. Carter, H. C. Bostock, A. Bolton, and E. Smith (2013), Southwest Pacific Ocean response to a warming world: Using Mg/Ca, Zn/Ca, and Mn/Ca in foraminifera to track surface ocean water masses during the last deglaciation, *Paleoceanography*, *28*, doi:10.1002/palo.20032.

1. Introduction

[2] The South Pacific Gyre (SPG) plays a dominant role in heat transportation, with surface currents transporting heat from the tropics to the subtropics. The SPG is also globally important as it links with other Southern Hemisphere midlatitude gyres in the Indian and Atlantic Oceans via the Tasman Leakage [*Ridgway and Dunn*, 2007; *Roemmich*, 2007]. Recent climatic warming has been accompanied by increased wind stress curl over the South Pacific. This has resulted in a "spin up" of the SPG, causing the poleward advance of the extended East Australian Current [*Ridgway and Hill*, 2009]. However, the degree to which traditional paleoceanographic methods can investigate past SPG change, as reflected in the surface oceans, is limited, restricting our understanding of the dynamic southwest Pacific Ocean environment.

[3] Previous work has indicated that the SPG contracted during the glacial, with a northward shift of the Subtropical Front (STF) [*Passlow et al*., 1997; *Sikes et al*., 2009]. The exception to this is along the Chatham Rise, east of New Zealand, where the STF is constrained by the topography and confined within 1–2° latitude [*Sikes et al*., 2002]. Evidence from eastern New Zealand suggests, however, that there may have been some flow-through of cold subantarctic surface waters (SAW) across the western end of Chatham Rise through the Mernoo Saddle (Figure 1) [*Weaver et al*., 1998; *Nelson et al*., 2000].

[4] This paper first endeavors to develop new paleoceanographic proxies using trace element geochemistry of planktic foraminifers, which may aid in our understanding of surface water masses. In situ measurements of Mg/Ca, Ba/Ca,

Additional supporting information may be found in the online version of this article.

[1]School of Geography, Environment and Earth Sciences, Victoria University of Wellington, Wellington, New Zealand.
[2]Antarctic Research Centre, School of Geography, Environment and Earth Sciences, Victoria University of Wellington, Wellington, New Zealand.
[3]National Institute of Water and Atmospheric Research, Wellington, New Zealand.
[4]Earth Observatory of Singapore, Nanyang Technological University, Singapore.

Corresponding author: H. C. Bostock, National Institute of Water and Atmospheric Research, PO Box 14-901 Greta Point, Wellington, 6241 New Zealand. (Helen.Bostock@niwa.co.nz)

©2013. American Geophysical Union. All Rights Reserved.
0883-8305/13/10.1002/palo.20032

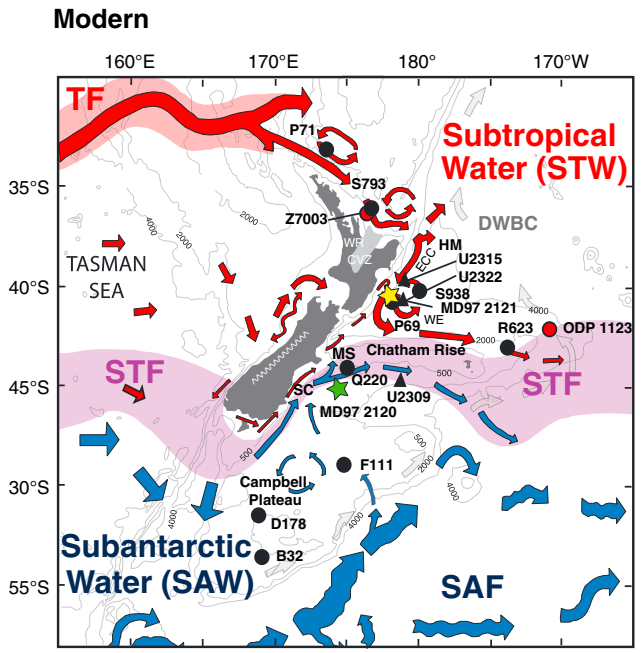

Figure 1. Generalized modern surface ocean currents and bathymetry surrounding New Zealand (modified from *Carter et al.* [2008]). Black and red circles mark the core top sites, with red sites denoting those used for *G. ruber* only. Plankton tow locations (black triangles), MD97 2121(yellow star), MD97 2120 (green star), and Southern Alps (white carets). TF, Tasman Front; STF, Subtropical Front; SAF, Subantarctic Front; ECC, East Cape Current; STW, Subtropical Surface Water; SAW, Subantarctic Surface Water; MS, Mernoo Saddle; WE, Wairarapa Eddy; CVZ-Central volcanic zone; WR, Waihou River; DWBC, Deep Western Boundary Current; HM, Hikurangi Margin. Isobaths are in meters.

Zn/Ca, and Mn/Ca in *Globigerina bulloides* (*G. bulloides*) and *Globigerinoides ruber* (*G. ruber*) were obtained using laser ablation inductively coupled plasma mass spectrometry (LA-ICPMS). Modern variations in foraminiferal core top and plankton tow trace metal concentrations are initially used to determine whether any distinctive chemical signatures could be used to distinguish between water masses [e.g., *Lea and Boyle*, 1991; *Marchitto et al.*, 2000]. These modern samples span a wide range of temperature and nutrient concentrations, and build on previous work that established regional calibration curves for foraminiferal Mg/Ca and ocean temperatures [*Bolton et al.*, 2011; *Marr et al.*, 2011].

[5] In situ trace element measurements are then presented for foraminifera from the last 25 ka of core MD97 2121 in the southwest Pacific Ocean (Figure 1) located north of the modern STF, at the southern boundary of the SPG. We used this record to assess whether any changes in the water mass, including surface water thermal and nutrient stratification at the MD97 2121 site, were recorded and preserved in the foraminiferal geochemistry. These novel geochemical water mass tracers are then used help enhance our understanding of how frontal surface waters of the SPG—in this case subtropical (STW) and SAW surface waters near the STF—responded since the last glacial, expanding upon the findings of previous studies in the region.

2. Background

2.1. Trace Metal Signatures in Foraminiferal Calcite

[6] The incorporation of trace metals into foraminiferal calcite is likely to be influenced by the waters from which the organisms calcify [e.g., *Hönisch et al.*, 2011]. Here we focus on Mg/Ca, which is now well established as a temperature proxy [e.g., *Anand et al.*, 2003; *Cléroux et al.*, 2008], and Zn/Ca, Mn/Ca, and Ba/Ca as potential paleowater mass and environmental tracers.

[7] Previously, Zn/Ca and Ba/Ca have been used as paleotracers in benthic foraminifera [*Lea and Boyle*, 1990; *Marchitto et al.*, 2000] and Ba/Ca in planktic foraminifera to track surface water changes in trace metal composition caused by changing fluvial input or upwelling [*Hall and Chan*, 2004; *Lea and Boyle*, 1991]. However, values of Ba/Ca in planktic foraminifera are typically low (approximately 1–15 µmol/mol), making it challenging to measure statistically significant offsets in test calcite where a Ba-enriched fluvial source is absent [*Hall and Chan*, 2004; *Lea and Spero*, 1994; *Weldeab et al.*, 2007]. Also, the use of oxidative or reductive cleaning procedures prior to the measurements of Zn/Ca, Mn/Ca, and Ba/Ca via solution-based analytical techniques can lead to marked differences in measurements [*Marr et al.*, 2013].

[8] Zinc and Mn are essential to biological processes associated with the primary productivity and enzymatic activity of phytoplankton [*Bruland and Lohan*, 2003; *Croot and Hunter*, 1998; *Lea and Boyle*, 1991; *Morel and Price*, 2003; *Price and Morel*, 1990]. They are collectively referred to as "bioactive trace metals" [*Bruland and Lohan*, 2003]. The mechanisms by which planktic foraminifera incorporate and mediate Mn, Zn, or Ba into test calcite are, however, unclear.

[9] There are various factors known to influence Mg incorporation, and which may also affect the other trace metals. Studies using in situ analytical techniques highlight the effect of day-night, high-low Mg/Ca banding through foraminifera test wall caused by light on symbiotic species [*Eggins et al.*, 2004; *Sadekov et al.*, 2005; *Spero et al.*, 2008]. While this can cause Mg/Ca offsets between calcite layers of up to 8 mmol/mol in species such as *Orbulina universa*, which precipitates approximately 30% of its shell as high-Mg/Ca calcite [*Spero et al.*, 2008], high-Mg calcite precipitation is significantly less in other species such as *G. ruber* [*Sadekov et al.*, 2008; *Sadekov et al.*, 2005]. *G. bulloides* is asymbiotic and there is no apparent high-low banding of Mg/Ca, Mn/Ca, Ba/Ca, or Zn/Ca through test walls associated with ontogenic growth as revealed by LA-ICPMS profiles through test walls [*Marr et al.*, 2013; *Marr et al.*, 2011]. LA-ICPMS also enables the direct targeting of specific chambers for trace metal analysis and thus allows assessment of changes in trace metal concentrations of different chambers during the foraminifera's lifecycle.

2.2. Surface Ocean Trace Metal Concentrations

[10] Differences in concentrations of Zn and Mn in the surface waters have been observed across the modern STF in the South Pacific Ocean. Mean dissolved Zn levels of 0.22 nmol/kg in STW are higher than a mean of 0.04 nmol/kg in SAW (M. Ellwood, personal communication, 2011). STW Mn concentrations are approximately

1.2 nmol/kg, while those from SAW generally range from 0.3 to 0.7 nmol/kg [*Klinkhammer and Bender*, 1980]. Thus, an increasing influence of nutrient-rich STW may potentially be indicated by elevated Zn/Ca or Mn/Ca in foraminifera.

[11] Dissolved Ba concentrations, however, are relatively homogenous with as little as 10–20% difference between SAW and STW off southern Australia [*Jacquet et al*., 2004]. While there is no major upwelling in this region to enhance Ba concentrations, there are many rivers that discharge along the lower eastern North Island, annually carrying approximately 83 Megatonnes of suspended load to the continental shelf [*Hicks and Shankar*, 2003]. The Waihou River, where the Mn and Zn concentrations have been measured, is the closest river to the core site MD97 2121, over 300 km to the northwest (Figure 1). The Waihou does, however, drain a similar catchment to rivers discharging into Hawke Bay (Figure 1). The Waihou River has dissolved Mn levels of 1.4–8.8 μg/kg and Zn of <0.1 μg/kg [*Webster*, 1995], lower than the global averages for sea water of 34 and 0.6 μg/L, respectively [*Gaillardet et al*., 2003]. Unfortunately, no dissolved Ba concentrations from rivers are available for the North Island of New Zealand (see supporting information).

2.3. Physical Oceanography

[12] The East Australian Current (EAC) is the main western boundary current of the SPG [*Ridgway and Hill*, 2009]. The EAC flows south along eastern Australia, with a component detaching to form the eastward flowing Tasman Front (TF) [*Ridgway and Dunn*, 2007]. This frontal flow attaches to northern New Zealand as the East Auckland Current and its southward continuation as the East Coast Current (ECC) continues to Chatham Rise before being steered eastward [*Ridgway and Hill*, 2009; *Tilburg et al*., 2001]. Seaward of the ECC is the anticyclonic, warm-core Wairarapa Eddy (WE) associated with the East Cape Eddy system. Eddies shed near East Cape and propagate southwest along the continental margin to Hawke Bay where they may stall or merge with a previous perturbation to form the WE [*Chiswell*, 2005; *Roemmich and Sutton*, 1998].

[13] South of Chatham Rise, the inflow to southern New Zealand is dominated by the Antarctic Circumpolar Current (ACC), whose leading edge is the Subantarctic Front (SAF). The SAF separates SAW from the colder Circumpolar Surface Water and is forced south around the bathymetric barrier of Campbell Plateau (Figure 1) [*Heath*, 1985; *Morris et al*., 2001].

[14] These subtropical and subantarctic inflows create a dynamically driven modern surface ocean east of New Zealand (Figure 1). The boundary between the two inflows is the STF positioned along the east-west crest of the Chatham Rise [*Chiswell*, 2002]. The front separates warm, saline, micronutrient-rich, macronutrient-poor STW in the north from cold, less saline, micronutrient-poor, macronutrient-rich SAW to the south [*Boyd et al*., 1999; *Ellwood et al*., 2008; *Locarnini et al*., 2006].

[15] Off the eastern South island, the STF is represented by the northward flowing Southland Current. At Chatham Rise, a branch of the Southland Current extends east to the STF, whereas another branch continues north through the Mernoo Saddle (Figure 1). On its passage north through the Mernoo Saddle, cool (~7°C), low-salinity (~34.6 practical salinity unit) Subantarctic Mode Water is forced from 580–800 m water depth to at least 275 m, and probably to the surface, via episodic wind-induced upwelling [*Heath* 1972a, 1972b; *Heath*, 1985; *Morris et al*., 2001].

3. Samples and Methods

3.1. Samples

[16] Modern foraminifera were sampled from 11 core top sites and three plankton tows spanning 20° of latitude, three water masses, and water depths from 580 to 3003 m (Figure 1). The deepest sites are close to the calcite saturation horizon, which locally lies at 2800–3100 m [*Bostock et al*., 2011]. Accordingly, individual foraminifera from core-top sites >2500 m depth were examined visually and via scanning electron microscopy for signs of test dissolution, which can indicate that preferential leaching of trace elements [e.g., *Brown and Elderfield*, 1996]. Any individuals that were potentially compromised by dissolution were removed from the data set.

[17] Ancient foraminifera were sampled from the upper 9.15 m, corresponding to the last approximately 25 kyr of giant piston core, MD97 2121, situated north of the modern STF (40°22.935′S, 177°59.68′E) at a water depth of 2314 m [*Carter et al*., 2008]. The oceanographic setting, high-sedimentation rate (29–42 cm/kyr), and well-constrained chronology [*Carter et al*., 2008] make this an optimal site to test these new geochemical proxies and learn more about the SPG over the last glacial/interglacial cycle.

[18] The samples were taken in approximately 5–10 cm intervals yielding an approximately 300–600 year resolution [e.g., *Carter et al*., 2008]. *G. ruber* and *G. bulloides* from core tops and MD97 2121 were handpicked from the 250–450 μm sieved fraction (Figure 2). *G. bulloides* is present continuously throughout the glacial-interglacial record; however, *G. ruber*, which favors warmer waters, is rare during the cooler intervals and is only present in sufficient abundance for analysis from circa 15.5 ka to the late Holocene.

3.2. Analytical Techniques

[19] Foraminifera were cleaned and mounted on a National Institute of Standards and Technology (NIST) 610 silicate glass standard for trace element analysis by LA-ICPMS following the protocols outlined in *Marr et al*. [2011]. Trace element/Ca ratios of foraminiferal tests were analyzed using a New Wave deep-UV (193 nm) solid-state laser ablation system coupled to an Agilent 7500CS ICPMS at Victoria University of Wellington, New Zealand. Monitored isotopes were ^{24}Mg, ^{27}Al, ^{43}Ca, ^{55}Mn, ^{66}Zn, ^{88}Sr, and ^{138}Ba. Laser ablation analyses were between 60 and 120 s in duration, depending on test wall thickness and/or density, to ensure consistent penetration of the *G. bulloides* and *G. ruber* test wall [e.g., *Marr et al*., 2011]. After subtraction of background signals, trace element/Ca ratios were calculated by reference to bracketing LA-ICPMS analyses of the NIST 610 glass standard and normalization to the preferred trace element values in this standard: Mg (465 ppm), Al (10,798 ppm), Ca (82,191 ppm), Mn (485 ppm), Zn (456 ppm), Sr (516 ppm), and Ba (435 ppm) [*Pearce et al*., 1997]. Analyses of NIST 610 were bracketed every 5–20 analyses of foraminifera and showed no significant drift in trace element/Ca ratios beyond the internal precision of the analyses over the course of the analytical sessions. The internal precisions (% 2 standard error)

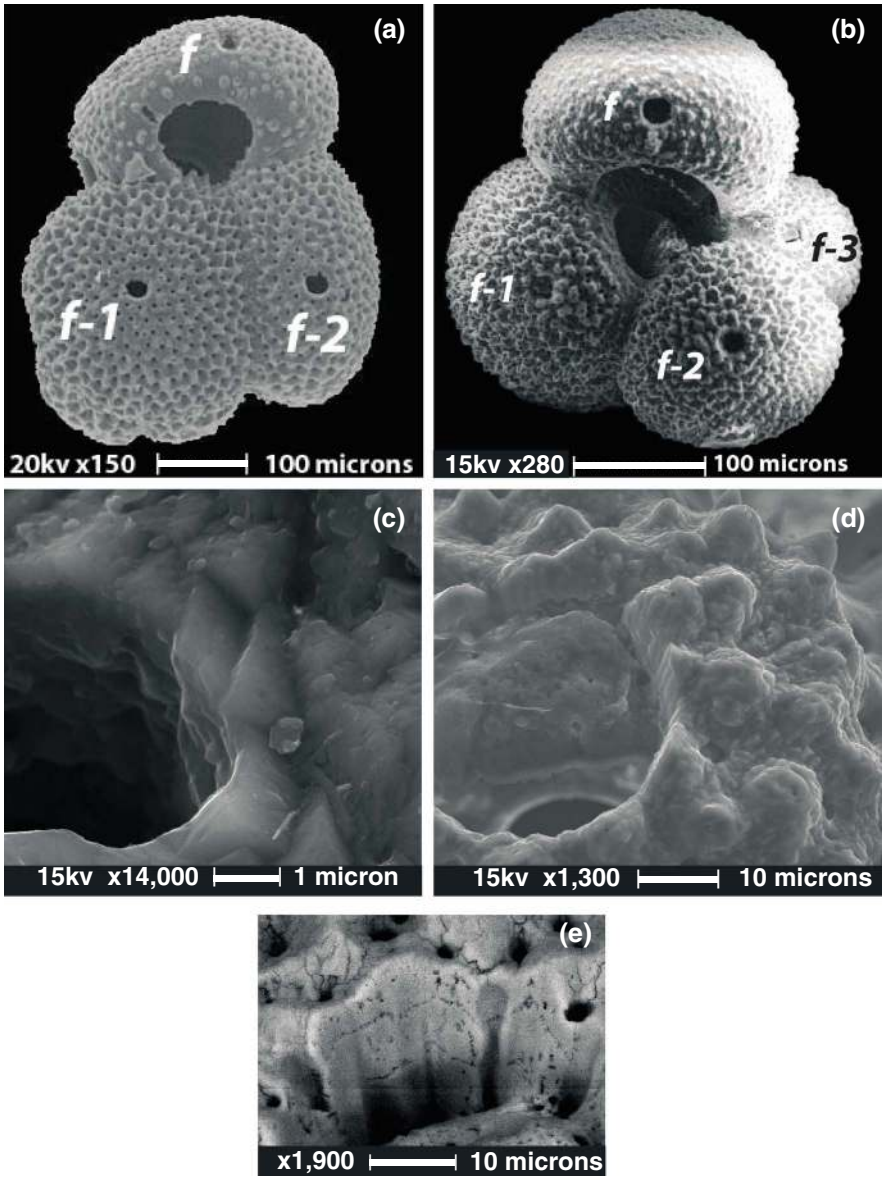

Figure 2. Scanning electron microscopic image of (a) *Globigerinoides ruber* and (b) *Globigerina bulloides*. The chambers are labeled such that *f* represents the final (youngest) chamber, *f-1* is the penultimate chamber, *f-2* is the antepenultimate chamber, and *f-3* the oldest chamber analyzed. Core top study results for mean STW and SAW trace element/Ca values are based on the mean of *G. bulloides* chambers *f-3*, *f-2*, and *f-1* values as this species is present in both STW and SAW. For the down core MD97 2121 record, only chambers *f-2* and *f* were analyzed for *G. bulloides* and chamber *f-2* for *G. ruber*. Laser ablation pits measuring 25 μm in diameter are visible. High-magnification images of pore space and surrounding calcite in a (c) glacial and (d) Holocene ablation pit *G. bulloides* show no change in calcification through the test wall which indicates little to no dissolution and/or re-crystallization has taken place. (e) Ablation pit through *G. bulloides* from another southwest Pacific location on which dissolution is clearly evident by the absence of thin calcite layers through the test wall.

of trace element/Ca ratios for a single foraminiferal analysis are typically as follows: Mg/Ca ± 1.0–2.5%, Al/Ca ± 5–20%, Mn/Ca ± 3–15%, Zn/Ca ± 6–23%, Sr/Ca ± 1.0–2.0%, and Ba/Ca ± 3–30%.

[20] Previous LA-ICPMS studies of foraminifera demonstrated that trace element depth profiles through a test wall are typically variable with a "surface veneer" enriched in Mg and other trace elements (except Sr) and similar, highly localized enrichment in Mg and other trace elements as the laser penetrates the inner test wall [e.g., *Eggins et al*., 2003; *Marr et al*., 2013]. This is especially true of Mn/Ca levels in foraminiferal calcite, which is known to be susceptible to postdeposition alteration [e.g., *Boiteau et al*., 2012; *Boyle*, 1983]. Careful scrutiny of the time-resolved trace element depth profiles during processing, with exclusion of high Mn/Ca phases potentially representing postdepositional contamination or diagenesis [e.g., *Boyle*, 1983], ensures that only primary calcite is represented in sample means [*Bolton and Marr*, 2013; *Marr et al*., 2011].

[21] For the modern core tops, all four visible chambers of *G. bulloides* and chamber *f-2* of *G. ruber* were analyzed [*Bolton et al*., 2011]. However, only data from *G. bulloides* older three visible chambers (*f-3* to *f-1*) were used to determine the mean for the water mass, as final chamber (*f*) values show a large offset from these older chambers [*Marr et al*., 2011]. Individual foraminifera values are grouped and presented as sample means for core top and plankton tows ($n = 10$–37) to allow comparison with studies that use solution techniques [e.g., *Anand et al*., 2003; *Pahnke and Sachs*, 2006; *Pahnke et al*., 2003].

[22] For the MD97 2121 down core samples, only the antepenultimate (*f-2*) and final (*f*) chambers of *G. bulloides* were analyzed, because chamber *f-2* yielded better within-chamber reproducibility than older *f-3* or younger *f-1* chambers and avoided issues associated with the kummerform chambers (Figure 2) [*Berger*, 1971]. Each sample mean (using chambers *f-2* or *f*) were composed of measurements from 10 to 46 individual specimens with the 95% confidence interval describing the distribution of the data about the sample mean given in supporting information Text S1. The term "Mg/Ca-temperatures" indicates temperatures which have been inferred from the Mg/Ca ratios. The variance of values in each sample was also calculated. Paleotemperature estimates were determined as follows:

G. bulloides—Mg/Ca (mmol/mol) = $0.952\ (\pm 0.041) \times e^{0.068\ (\pm 0.002) \times T}$ ($r^2 = 0.95$), calibrated temperature range approximately 7.0–31.0°C [*Marr et al*., 2011];

G. ruber—Mg/Ca (mmol/mol) = $0.798\ (\pm 0.133) \times e^{0.070\ (\pm 0.005) \times T}$ ($r^2 = 0.89$), calibrated temperature range approximately 14.0–29.0°C [*Bolton et al*., 2011].

4. Results

4.1. Mn/Ca, Zn/Ca, and Ba/Ca Ratios in the Modern Ocean

[23] Mn/Ca and Zn/Ca typically occur in low (<300 μmol/mol) and Ba/Ca in ultralow (<10 μmol/mol) levels in the modern and ancient foraminifera studied here (Figures 3–6 and Table 1) [e.g., *Lea and Boyle*, 1991; *Rosenthal et al*., 1999]. Individual LA-ICPMS analyses of these elemental ratios can have large uncertainties due to low concentrations of Mn, Zn, and Ba and heterogeneity of the foraminiferal test wall. Multiple analyses ($n = 3$–5) of single chambers of an individual foraminifera show that the external reproducibility (2 standard deviation) of trace element/Ca ratios for a single foraminifera analysis is better than Mn/Ca ± 15–60% (±9–33 μmol/mol), Zn/Ca ± 14–52% (±4–19 μmol/mol), Ba/Ca ± 27–157% (±2–14 μmol/mol). Some of this variability represents real heterogeneity within the foraminiferal test chambers and overestimates the analytical external reproducibility [*Marr et al*., 2011]. Nevertheless, the Mn/Ca and Zn/Ca mean values of *G. bulloides* from STW core top sites are statistically different from SAW core top sites ($Mn/Ca_{STW} = 23.7$–120.2 versus $Mn/Ca_{SAW} = 1.8$–7.6 μmol/mol and $Zn/Ca_{STW} = 19.7$–65.6 versus $Zn/Ca_{SAW} = 7.5$–14.1 μmol/mol). The relative differences of these mean elemental ratios from *G. bulloides* between STW and SAW core top sites, approximately 1700% for Mn and 400% Zn, are larger than analytically or known biologically induced uncertainties (Figure 3).

[24] *G. bulloides* and *G. ruber* mean Zn/Ca and Ba/Ca values from individual core top and plankton tow samples are in good agreement, suggesting that any postdepositional alteration of tests is not significant (Figure 3, Table 1, and supporting information Text S2) for these elements. However, mean Mn/Ca of 0.6 μmol/mol measured on the *G. bulloides* from U2309 plankton tow is 4–12 times lower than that of nearby core tops. Likewise, the mean Mn/Ca of 7.6 μmol/mol measured on *G. ruber* from plankton tows U2315 and U2322 from STW is five times less than that from adjacent core top ratios (Table 1 and supporting information Text S2).

[25] Mean Mn/Ca and Zn/Ca ratios for modern *G. bulloides* compared across all core top and plankton tow samples show approximately an order of magnitude variation, with the largest difference evident across the STF (Figures 1–3 and Table 1). *G. bulloides* Zn/Ca values from STW sites are four times greater than their SAW counterparts (Figure 3). This broadly mirrors modern water chemistry, where the mean STW Zn levels are >5 times higher than in SAW (Figure 3g) (M. Ellwood personal communication, 2011). *G. bulloides* STW and SAW foraminiferal Mn/Ca values also mimic the distinctive water mass trace metal concentrations, where particulate STW Mn is two to four times higher than that found in SAW south of Australia (Figure 3d) [*Bowie et al*., 2009]. *G. bulloides* Ba/Ca from SAW and STW does not vary significantly between samples, which are very low (0.5–5 μmol/mol) for distal sites P71, B32, D178, and F111, dominated by carbonate-rich sediments (Figure 3c). However, core top and plankton tow Ba/Ca results from S938, R623, and U2309 have values of up to 8.7 μmol/mol, and S793 up to 14 μmol/mol or 400% higher (Figure 3c). Corresponding enrichments or depletions in foraminiferal Zn/Ca, Mn/Ca, or Mg/Ca are not apparent in these same samples.

[26] *G. ruber* samples are restricted to the warmer STW; however, their mean Mn/Ca, Zn/Ca, and Ba/Ca values are similar to those for *G. bulloides* older chambers *f-3*, *f-2*, and *f-1* from the same or nearby sites (ODP1123:R623, Z7003:S973, P71) (Figure 3 and Table 1).

[27] Modern *G. bulloides* chamber *f* values tend to be more enriched in Zn/Ca than either *G. bulloides* chambers *f-1* to *f-3* by up to 40% or in *G. ruber* (chamber *f-2*) by up to 50% (Table 1). The difference between *G. bulloides* chamber *f* and *G. ruber chamber f-2* is generally up to 50%, except the data from plankton tow sites U2322 and U2315. At these two plankton tow sites *G. ruber* Zn/Ca values are more than 50% higher than core top sites which suggests that these samples may contain some remnant Zn-enriched organic material (Figure 3). The relationship between *G. bulloides* chamber *f* and *G. ruber* chamber *f-2* Zn/Ca may replicate the modern surface water concentration gradients, where Zn/Ca is approximately 50% higher at 100 m depth than at 30–40 m (Figures 3h and 3i) [*Martin et al*., 1989].

[28] All *G. bulloides* chambers and *G. ruber* Mn/Ca values from the same sample are indistinguishable (P71; Table 1). Ba/Ca is present in ultralow concentrations, and any interchamber variations are close to uncertainty; however, the general trend is for *G. bulloides* older chambers *f-3*, *f-2*, and *f-1* and *G. ruber* to be more enriched in Ba/Ca than *G. bulloides* chamber *f* (Table 1).

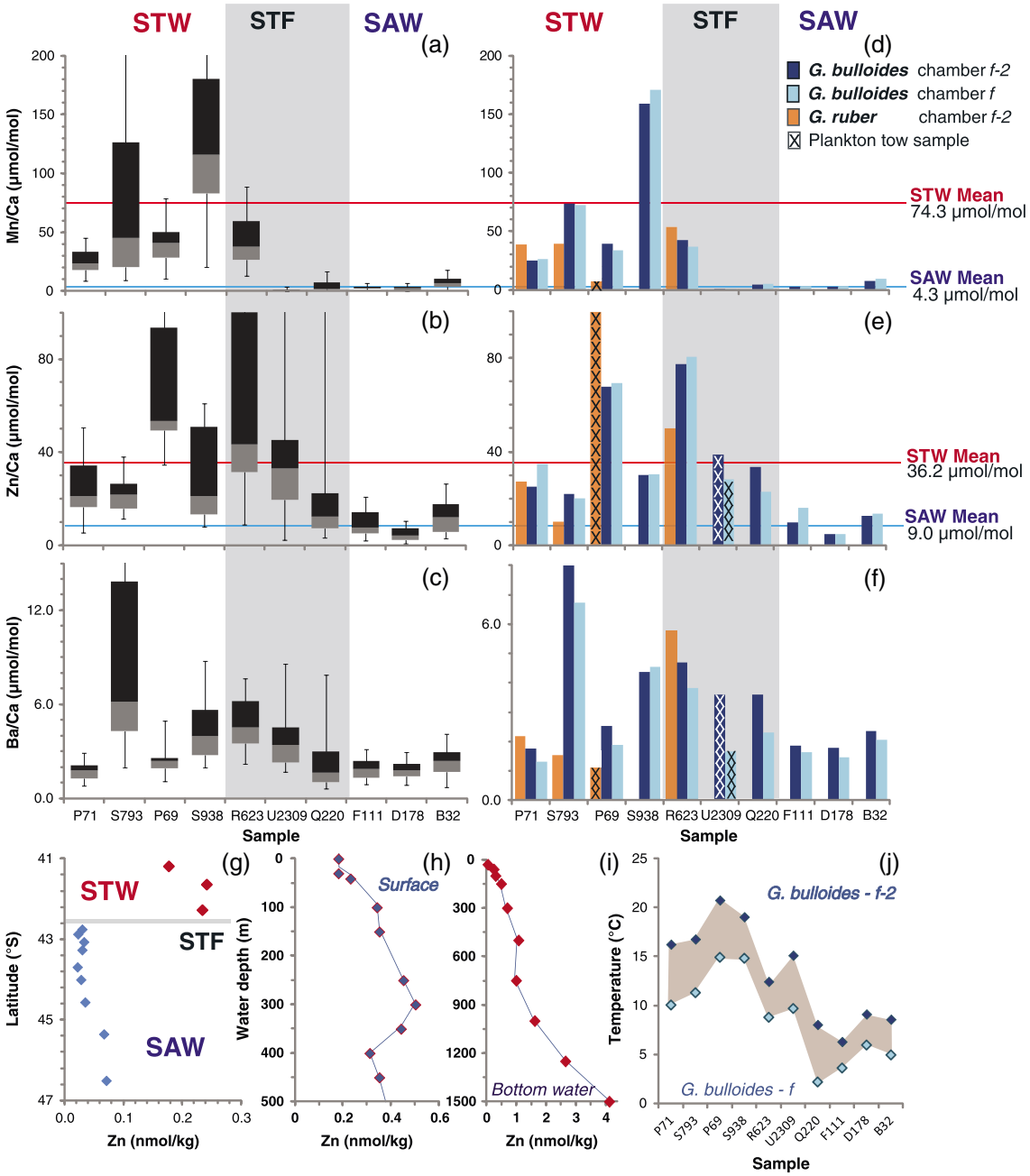

Figure 3. Comparison of sample trace element/Ca ratios for modern *G. bulloides* chambers *f-1* to *f-3* (inclusive) and *G. ruber* chamber *f-2* with each sample mean composed of measurements from multiple individual specimens. Core sites are presented according to their respective latitudes (Table 1) from north to south with those sites from the STW and SAW indicated either side of the STF sites (grey-shaded box). (a–c) "Box and whisker" plots illustrate values of all *G. bulloides f-2* analyses at a given site. (d–f) Bar graphs represent *G. ruber* (orange) and *G. bulloides* (chambers *f-3-1*—dark blue; chamber *f*—light blue). Note *G. ruber* site Z7003 has been incorporated into S793 and ODP1123 into R623 due to their close proximity. The bar graph indicates mean site values for *G. bulloides* chambers *f-1–f-3* (dark blue) and *f* (light blue). The Zn/Ca and Mn/Ca solid lines represent the mean values for the STW (P71, P81, S793, P69, and S938—red) and SAW (F111, D178, and B32—blue) sites. Site means are for *G. bulloides* chambers *f-1* to *f-3* only. Plankton tow values from U2309 (*G. bulloides*) and U2315 and U2322 (*G. ruber*) are indicated by hashed lines. Note *G. ruber* plankton tow values have been appended to site P69 due to location proximity. (g) STW and SAW water mass Zn concentrations sampled in October 2000 (M. Elwood, unpublished data, 2012) approximately 41.2°S–46.5°S, 178.5°E–178.6°E. (h) Zn surface water concentrations from 0 to 500 m and (i) surface to deep water from 0 to 1500 m, 39.47°S, 179.35°E (M. Elwood, unpublished data, 2012). (j) Modern surface ocean thermal stratification as measured by Mg/Ca thermometry of *G. bulloides* chamber *f-2* (solid dark blue diamonds) and *f* (open dark blue diamonds).

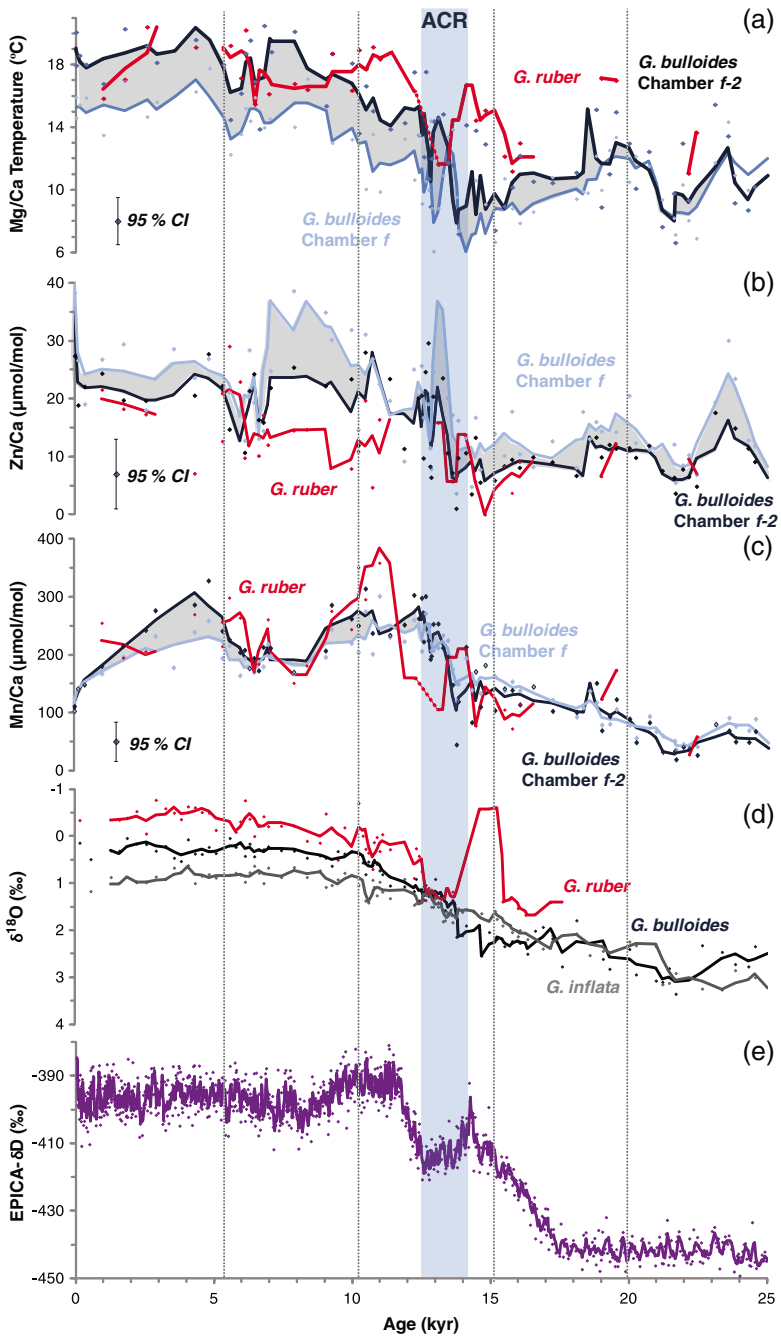

Figure 4. Geochemical and isotopic proxy data from (a–d) MD97 2121 and (e) Antarctica for the last 25 kyr. Laser ablation ICPMS data (this study, Figures 4a–4c) are shown for two chambers of *G. bulloides* as the dark blue line—*f-2* (antepenultimate chamber) and light blue line—*f* (final chamber) with each sample mean composed of measurements from multiple individual specimens. Data for *G. ruber* (red line) are from laser ablation analyses of chamber *f-2*. Mg/Ca temperatures using the calibrations of *Marr et al.* [2011] and *Bolton et al.* [2011], Zn/Ca nutrient stratification, Mn/Ca productivity, $\delta^{18}O$ profiles of three planktic foraminiferal species from the MD97 2121 record [*Carter et al.*, 2008], European Project for Ice Coring in Antarctica Dome C deuterium record [*Jouzel et al.*, 2007]. The timing of the Antarctic Cold Reversal (ACR) is indicated by the blue-shaded bar. Grey-shaded area highlights the difference in trace metal values between *G. bulloides* chambers *f* and *f-2*. Geochemical data are presented using a three-point moving mean for trend comparison with typical 95% confidence interval (CI) about the moving mean shown as error bars to simplify the graph. Individual sample values are represented as points on the graph. Where the density of data is less than two samples/3 ka, no trend line has been drawn. Dashed red line from 13.5 to 12.5 kyr indicates a period of appreciable variability evident in *G. bulloides* data for which *G. ruber* record is absent, likely due to an influx of SAW water which is also evident in the faunal assemblage record (Figure 4e).

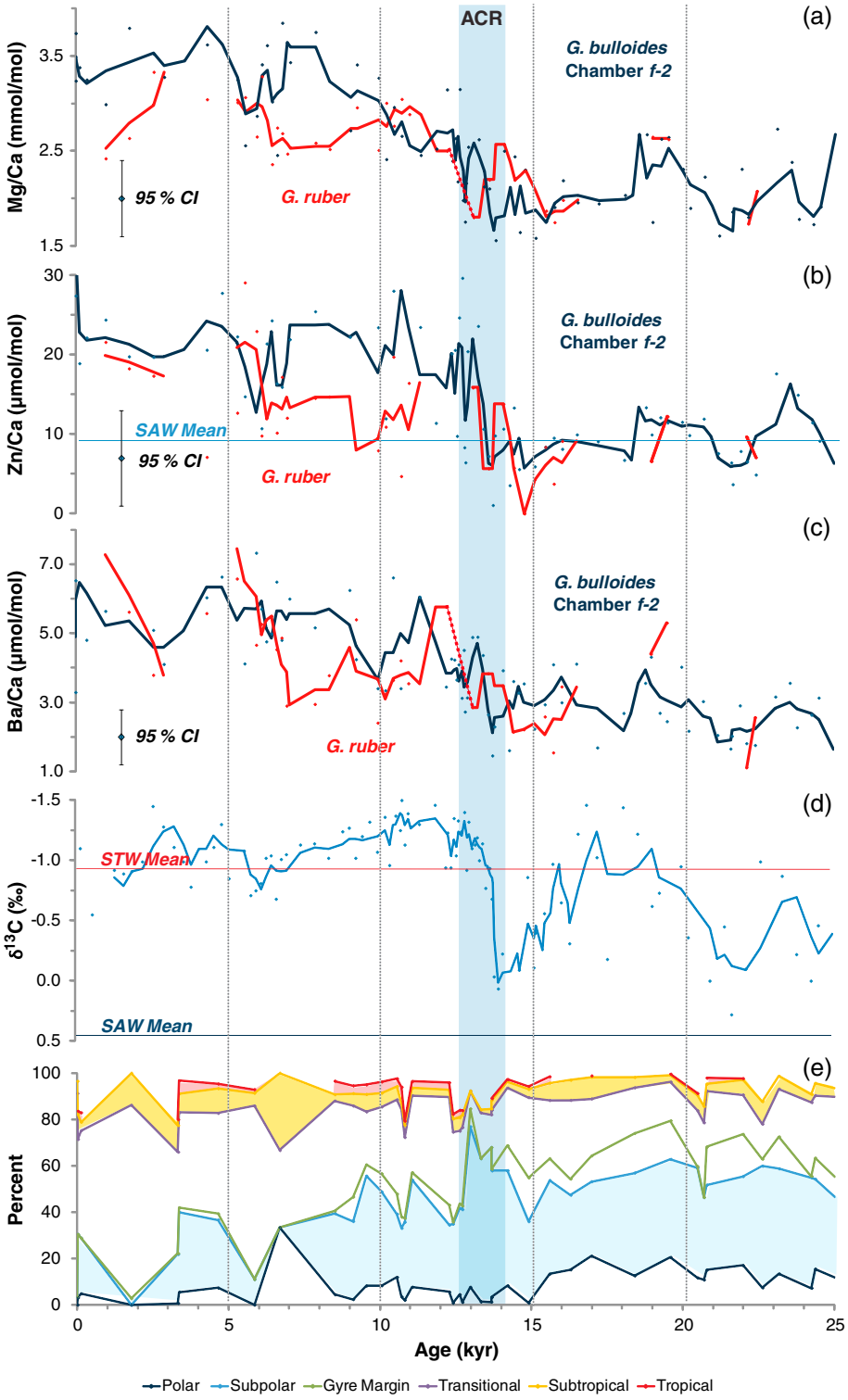

Figure 5. (a) Mg/Ca, (b) Zn/Ca, and (c) Ba/Ca records of core MD97 2121 for the past 25 ka for *G. ruber* (red) and *G. bulloides* (blue) with each sample mean composed of measurements from multiple individual specimens. Horizontal blue and red lines on the graph define SAW and STW water mass modern trace element/Ca means as determined from modern core top analyses (from Figure 3). Also presented is the (d) $\delta^{13}C$ record for *G. bulloides* (blue) [*Carter et al.*, 2008] together with mean values of 0.51 and −0.95 for SAW and STW, respectively, are from repeat core top *G. bulloides* analyses undertaken at NIWA and (e) the foraminiferal assemblages of species with known environmental preferences [*Imbrie and Kipp*, 1973], based on samples of >100 individuals [*Northcote et al.*, 2007]. The timing of the Antarctic Cold Reversal (ACR) is indicated by the blue-shaded bar. See Figure 4 for details on data presentation.

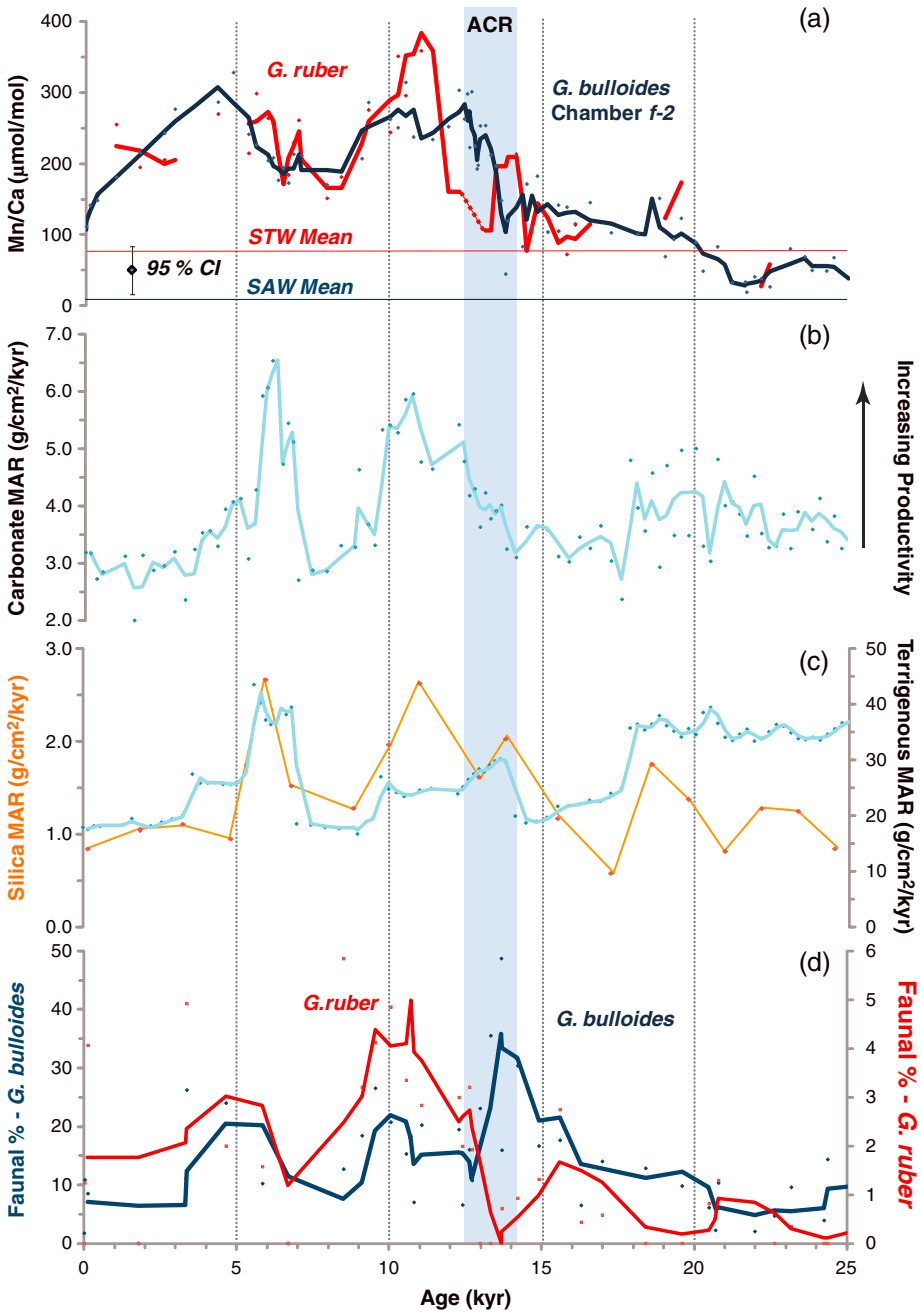

Figure 6. Geochemical, biogenic sediment-based productivity indicators for the MD97 2121 paleorecord and abundance of key faunal taxa. (a) Mn/Ca for *G. bulloides* (blue) and *G. ruber* (red). (b) Carbonate mass accumulation rate (MAR) and (c) terrigenous sediment and silica MARs for MD97 2121 [*Carter et al.*, 2008]. (d) Percentage of *G. ruber* (red) and *G. bulloides* (blue) from the total planktonic foraminifera species abundance, based on samples of >100 individuals [*Northcote et al.*, 2007]. The Antarctic Cold Reversal (ACR) is indicated by the blue-shaded bar. See Figure 4 for details on data presentation.

4.2. Glacial-Interglacial Mg/Ca, Zn/Ca, Mn/Ca, and Ba/Ca

[29] MD97 2121 core data (Figures 3, 4 and supporting information Text S1) show that the mean glacial Mg/Ca temperatures for *G. bulloides* (chamber *f-2*) and *G. ruber* (chamber *f-2*) are 10.4 and 12.4°C, respectively, from 25 to 21 ka. *G. bulloides* Mg/Ca records an initial temperature increase of approximately 4°C from circa 22 to 18 ka followed by an equivalent decrease in temperature from 18 to15 ka. From circa 17 to 14 ka, there is an apparent decoupling of *G. bulloides* and *G. ruber* surface ocean Mg/Ca temperature trends, while *G. ruber* indicates increasing temperatures, *G. bulloides* displays continued, but highly variable, decreasing temperatures (Figure 4). Significant, but erratic, warming of approximately 6–7°C is only indicated by *G. bulloides* Mg/Ca ratios after circa 14 ka during the Antarctic Cold Reversal (ACR; circa 14.2–12.4 ka) (Figure 4). Meanwhile, *G. ruber* Mg/Ca temperatures decrease by approximately

Table 1. Details of Core Top and Plankton Tow Locations, Water Depth, and Number of Foraminifera Analyzed From 12 Core Top and 3 Plankton Tow Site in the Southwest Pacific Ocean, East of New Zealand Used for Calibrating the Planktic Foraminifera Water Mass Proxies (Figure 1)[a]

Site	Water Depth (m)	*N*	Latitude (°S)	Longitude (°E)	Water Mass[b]	Mn/Ca (μmol/mol)	Zn/Ca (μmol/mol)	Ba/Ca (μmol/mol)	Mn/Ca (μmol/mol)	Zn/Ca (μmol/mol)	Ba/Ca (μmol/mol)
			G. bulloides				Chambers *f-3–f-1*			Chamber *f*	
P71	1919	18	33.86	174.69	STW	2.51	24.9	1.8	26.2	34.7	1.3
						5.2	*6.6*	*0.3*	*5.8*	*6.7*	*0.3*
S793	2411	18	36.32	176.80	STW	73.4	21.9	8.6	72.4	20.0	6.7
						33.6	*3.7*	*3.0*	*42.6*	*5.2*	*3.5*
P69	2195	14	40.40	178.00	STW	39.6	67.7	2.5	33.7	69.3	1.89
						10.9	*15.3*	*0.6*	*6.8*	*20.3*	*0.4*
S938	3003	12	40.03	180.00	STW	159.0	30.2	4.4	170.6	30.4	4.54
						79.9	*13.3*	*1.3*	*65.7*	*12.1*	*1.6*
R623	1128	16	43.20	186.00	STF: SAW/STW	42.7	77.5	4.7	36.9	80.7	3.8
						11.8	*36.9*	*1.0*	*7.8*	*38.0*	*1.0*
Q220	580	10	44.29	174.98	STF: SAW/STW	4.5	38.9	3.6	0.3	28.0	1.56
						0.3	10.0	0.5	0.1	6.0	0.2
[Δ]U2309	3585	37	46.40	178.30	STF: SAW/STW	0.6	33.3	2.7	5.2	22.8	2.3
						0.3	40.4	1.8	2.8	7.0	1.5
F111	704	22	48.95	174.98	SAW	2.8	9.8	1.9	3.4	15.8	1.63
						0.6	*2.6*	*0.3*	*0.8*	*3.6*	*0.3*
D178	629	19	51.72	169.83	SAW	2.6	4.6	1.8	3.4	4.7	1.48
						1.0	*1.5*	*0.3*	*1.4*	*1.3*	*0.3*
B32	799	23	53.63	169.87	SAW	7.6	12.6	2.4	9.7	13.4	2.05
						2.1	*3.0*	*0.4*	*2.4*	*3.0*	*0.4*
			G. ruber				Chamber *f-2*				
P71	1919	15	33.86	174.69	STW	38.9	27.2	2.2			
						14.3	*7.0*	*0.8*			
Z7003	430	18	36.69	176.24	STW	39.3	10.2	1.5			
						9.2	*4.9*	*0.4*			
[Δ]U2315		31	38.51	179.02	STW	7.6	103.7	1.11			
[Δ]U2322			41.60	178.05		*2.3*	*26.8*	*0.1*			
ODP1123	3290	13	41.94	188.50	STF: SAW/STW	53.5	49.9	5.8			
						37.6	*20.3*	*1.6*			

[a]Also presented is a summary of trace element chemistry for *G. bulloides* three oldest chambers (*f-1*, *f-2*, and *f-3*), final chamber (*f*), and *G. ruber* outlined here as sample means with 95% confidence interval in italics.
[b]STW = Subtropical Water; SAW = Subantarctic Water; STF = Subtropical Front [*Carter et al*., 2008]. Note that where subtropical mean or subantarctic water means have been presented, only those sites solely labeled STW or SAW have been used. For additional details about core top sites, see *Marr et al*. [2011].

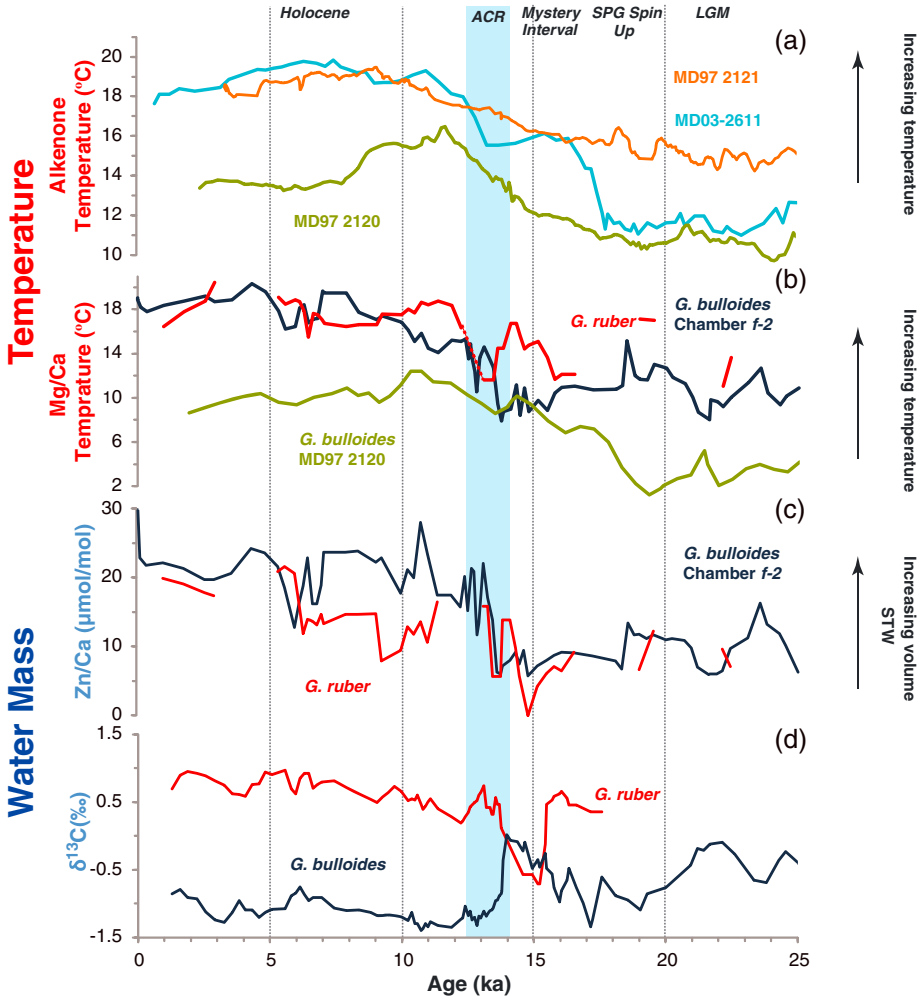

Figure 7. Compilation of regional water mass proxy data with other SW Pacific published data. Temperature proxy data includes (a) regional high-resolution alkenone data for site MD97 2121 [*Pahnke and Sachs*, 2006], for site MD03 2611 (South Australia) [*Calvo et al*., 2007], and site MD97 2120 (off the South Island, New Zealand) [*Pahnke et al*., 2003]; and (b) Mg/Ca temperature data *G. ruber* (red), *G. bulloides* (blue) in this study for MD97 2121, and for site MD97 2120 *G. bulloides* (green; Mg/Ca data from *Pahnke et al*. [2003] converted to temperature using calibration from *Marr et al*. [2011]). (c) Water mass proxies Zn/Ca *G. bulloides* (blue), *G. ruber* (red) for this study, and (d) $\delta^{13}C$ *G. bulloides* (blue), *G. ruber* (red) [*Carter et al*., 2008]. All geochemical data are presented using a three-point moving mean for trend comparison, except for MD97 2120 Mg/Ca and MD03 2611 alkenone data which are at a lower temporal resolution and therefore individual data points have been joined. The timing of the Antarctic Cold Reversal (ACR) is indicated by the blue-shaded bar.

4°C during the ACR. Mean Holocene *G. ruber* and *G. bulloides* (*f-2*) surface ocean Mg/Ca temperatures (17.9 and 17.8°C, respectively) are within error of each other and of modern regional surface ocean temperatures (Carter, unpublished report, 2000). However, circa 9–6.5 ka and again in the late Holocene (<3 ka) *G. bulloides* (chamber *f-2* Mg/Ca) records higher temperatures by up to 3°C than *G. ruber*, the opposite of normal species stratification.

[30] Previous laser ablation measurements of core top and plankton tow *G. bulloides* show that chamber *f* Mg/Ca values are approximately 20–30% lower than those of chamber *f-2* [*Marr et al*., 2011]. Down core *G. bulloides* chamber *f-2-f* offset varies markedly during the glacial period, including times when chamber *f* Mg/Ca temperatures are similar to, or occasionally higher than, those of the older chambers (Figure 4). During the ACR, there is little significant difference in Mg/Ca values between chambers. Following the ACR, the offset between chambers is relatively consistent, equivalent to 3–4°C throughout the Holocene (Figure 4).

[31] Glacial to Holocene Zn/Ca, Mn/Ca, and Ba/Ca trends of *G. bulloides* and *G. ruber* generally follow that of Mg/Ca (Figures 3 and 4) [*Carter et al*., 2008; *Weaver et al*., 1997]. In the glacial, the Zn/Ca values are similar to that from modern SAW core tops, while during the deglaciation, including the ACR, Zn/Ca values of *G. bulloides f-2* increase dramatically from 9.3 to 24.4 µmol/mol and Ba/Ca from 2.8 to 5.3 µmol/mol. *G. bulloides f-2* Mn/Ca values are lowest during peak glacial conditions at approximately 40 µmol/mol circa 23–22 ka, gradually increasing until the ACR when they peak at approximately 300 µmol/mol, and

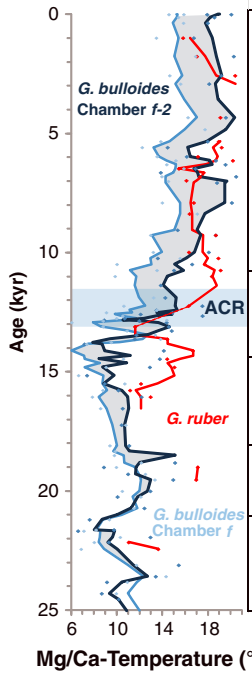

		Vertical Gradients	Inference Basis	Dominant Forcing	Comment
Holocene	11 ka - present	Generally well mixed at the surface with a well stratified subsurface. Nutrocline stratification well developed.	*G. bulloides* mean Mg/Ca and Zn/Ca values between chambers *f-2* and *f* are offset by *ca.* 0.7 mmol/mol and 7 µmol/mol respectively suggesting well developed stratification.	STW dominant with possible SAW pulse from *ca.* 5.5-7 ka.	Poleward migration of ocean fronts, with strengthened South Pacific Gyre (SPG) brings an increased inflow of STW. Perturbation towards lower temperatures and increased SAW inflow from *ca.* 5.5-7 ka a time of increased storminess [1].
ACR	14-12.5 ka	Limited stratification. Temperature decreases by up to 4 °C.	Convergence of chamber *f* and *f-1* Mg/Ca values of < 0.3 mmol/mol suggests reduced stratification.	SAW dominant, but possibly under increased winds periodic increased inflow of STW.	Interplay between SAW and STW reduces stratification and induces large shift in the surface water temperature profile.
MI	17.5-14.5 ka	*G. bulloides* temperature decrease by *ca.* 1°C/ka, but alkenones increase by *ca.* 0.5 °C/ka. Limited nutrient stratification.	Convergence of chamber *f* and *f-1* Mg/Ca and Zn/Ca values of < 0.2 mmol/mol and 3.5 µmol/mol respectively suggests reduced stratification.	SAW dominant with reduced inflow of STW.	Increased spring upwelling of cooler, nutrient depleted waters, coupled with higher summer insolation produced contrasting paleo-thermometer trends.
SPG Spin-up	22-18 ka	Limited stratification. Temperature *ca.* 2-4 °C higher than LGM.	Convergence of chamber *f* and *f-1* Mg/Ca of < 0.1 suggests reduced stratification.	SAW dominant with STW pulse.	SPG spin-up possibly due to northern hemisphere forcing [2]. No corresponding warming identified south of STF [3] or in Antarctic ice records [4].
LGM	25-21 ka	Limited temperature and nutrient stratification. Temperature *ca.* 6-7 °C lower than present.	Convergence of chamber *f* and *f-1* Mg/Ca and Zn/Ca of < 0.1 mmol/mol and 3.5 µmol/mol respectively suggests reduced stratification.	SAW dominant with reduced inflow of STW.	Mean sub-surface water temperatures *ca.* 6-7 °C lower than present. Diminished SPG. Increased windiness or ocean turbulence likely reduced surface water stratification.

Figure 8. Summary of surface water changes in the vertical gradients, inference basis, and dominant forcing from 25 ka to the present. MI = Mystery Interval, or period from 17.5 to 14.5 ka. Superscripted numbers 1: *Gomez et al.* [2012], 2: *Stuiver et al.* [1997], 3: *Lorrey et al.* [2012], and 4: *European Project for Ice Coring in Antarctica* [2004].

maintain a range of approximately 100–300 µmol/mol throughout the Holocene. Holocene mean *G. bulloides f-2* Zn/Ca values of 24.4 µmol/mol are similar to those of STW from core tops.

[32] Shallow-dwelling *G. ruber* records the lowest Zn/Ca values, whereas deeper-living *G. bulloides* has higher values, especially in chamber *f* (Figure 4). Glacial *G. ruber* and *G. bulloides f-2* Zn/Ca offsets and *G. bulloides* interchamber (*f-2-f*) Zn/Ca offsets are relatively consistent with *G. bulloides* chamber *f* more enriched in Zn/Ca by approximately 45% than chamber *f-2* (Figure 4). At the ACR, however, there is no offset in Zn/Ca values between chambers *f-2* and *f* in *G. bulloides* or *G. bulloides-G. ruber*. During the Holocene, the Zn/Ca offset between *G. Bulloides* and *G. ruber* is variable, reaching a peak difference between circa 10 and 6.5 ka when *G. bulloides* chamber *f* values double those of *G. ruber*.

[33] The variance of the trace element/Ca data within individual samples was also calculated. Mg/Ca variance of *G. bulloides* chamber *f-2* averaged 0.92 mmol/mol from 25 to 18 ka and 0.86 mmol/mol from 18 to 10 ka. From circa 10 ka, there is approximately 50% increased Mg/Ca variance, increasing to 1.37 mmol/mol, with a similar result for chamber *f*. The scatter was further tested over the delineated periods to ascertain if the difference in population variance was significant by the application of the "*F* test" [*Dixon and Massey*, 1969]. A value of $F = 1.09$ ($F\text{inv} = 1.74$, d.f. = 48) confirmed that the difference is significant. Similar variance trends were also found for Zn/Ca and Mn/Ca. *T* test values of 17.6 between the periods 25 and 14 ka, and 17.1 between 12.5 ka and present ($p < 0.05$, d.f. = 48) clearly indicate a significant difference.

5. Discussion

5.1. Zn/Ca, Mn/Ca, and Ba/Ca as Tracers of Ocean Change

[34] The evidence from the modern core tops and plankton tows suggests that these trace elements show distinct offsets between STW and SAW in the southwest Pacific. If modern Zn/Ca concentrations in surface waters (section 4.1 and Figure 3) hold for the paleocean record, Zn/Ca concentrations in *G. bulloides* and *G. ruber* chambers potentially can track surface water masses. Zinc is essential for phytoplankton photosynthesis and has a spatial and vertical distribution similar to those of the other micronutrients (Figure 3h). The results from modern core tops in this study suggest that Zn/Ca in fossilized foraminiferal calcite may also be a paleonutrient proxy.

[35] Manganese, after Fe, is the most important trace element for marine phytoplankton growth and is approximately 10 times more abundant in seawater than Zn (Figure 4) [*Ho et al.*, 2003; *Morel et al.*, 2003]. However, Mn/Ca ratios in foraminiferal test calcite are a conundrum. Core top data reveal a clear distinction between sites underlying SAW (mean 4.3 µmol/mol) and STW (mean 74.3 µmol/mol), suggesting a link with those water masses. Such low SAW values are confirmed by a plankton tow from the STF (U2309) where there is a strong SAW influence via the subantarctic-dominant Southland Current (Figure 1) [*Sutton*, 2003]. The down core variability suggests that change in measured Mn/Ca values is primarily a response to changing water masses. Minimum Mn/Ca values occur during the glacial, which is consistent with the dominance of SAW, as evinced by Mg/Ca, Zn/Ca, stable isotopes,

and foraminiferal assemblages (Figure 4) [*Carter et al*. 2008]. We discount any possibility of Mn/Ca being influenced by terrigenous input, as terrigenous flux increased in the glaciation when Mn/Ca is low at MD97 2121 (Figure 6) [*Carter and Manighetti*, 2006]. During the Holocene, Mn/Ca is generally higher than glacial values, again consistent with STW dominance as identified by aforementioned proxies [e.g., *Weaver et al*., 1998]. However, Holocene *G. bulloides* and *G. ruber* Mn/Ca is significantly elevated above the modern STW, and while the cause of this offset remains unknown, it raises the possibility of other influences (Figure 6 and supporting information). Several peaks in Mn/Ca occur during the Holocene, including a distinct peak in *G ruber* Mn/Ca centered on 11 ka. This coincides with a time of elevated carbonate and silicate mass accumulation rate (MAR) and warmer sea surface temperatures (SSTs) from the subtropic surface waters suggesting some influence of increase STW inflow and potentially productivity.

[36] In contrast to Zn/Ca and Mn/Ca, levels of Ba/Ca in the modern *G. ruber* and *G. bulloides* samples do not distinguish between STW and SAW. Core top S793 has elevated Ba/Ca levels, which may reflect locally high fluvial input [*Hicks and Shankar*, 2003]. However, foraminifera from other high fluvial inputs (P69, S938) do not have elevated Ba/Ca values (Figure 3), suggesting that fluvial discharge is not a primary control on local Ba concentrations (Figure 3). The higher Ba/Ca at S793 may also be due to the proximity to the volcanic hydrothermally active White Island (Figure 1), which produces rocks and hydrothermal fluids with high levels of Ba (rocks $>1000\,g/m^3$) [*Hedenquist et al*., 1993]. The MD97 2121 record reveals a small offset between glacial and interglacial Ba/Ca values, suggesting a change in Ba concentrations in the ambient water mass (Figure 5). However, as fluctuations of Ba/Ca are unlikely to reflect terrestrial sources as seen in the core top material, the reason for the offset is unresolved (Figure 3).

5.2. Thermal and Nutrient Stratification

[37] Modern *G. bulloides* chamber *f* is lower in Mg/Ca compared to the previous chambers. This is likely to reflect a lower temperature at the time the chamber was calcified, an interpretation consistent with this species migrating to deeper depths near the end of its lifecycle (Figure 3i) [*Hemleben et al*., 1989; *Marr et al*., 2011]. Alternative reasons for offsets in Mg/Ca and other trace metal values between chambers may include diagenesis disproportionally affecting the thinner chamber *f*. However, diagenesis seems unlikely as Mg/Ca values (and therefore Mg/Ca paleotemperatures) decrease in chamber *f* relative to chamber *f-2*, while Zn/Ca values increase and Mn/Ca remains relatively unchanged (Figure 4). *G. bulloides* Mg/Ca mean and chamber *f* values for core tops adjacent to the plankton tows are also consistent with the change in trace metal values originating from primary calcite (Figure 3).

[38] Core top Mg/Ca-temperature data for *G. bulloides* reveal a systematic offset with final chamber (*f*) consistently yielding lower temperatures (Figure 3). The final chamber Mg/Ca temperatures are approximately 5.5°C (STW core tops) and 3°C (SAW core tops) colder than corresponding chamber *f-2* estimates for *G. bulloides* (Figure 3i) [*Marr et al*., 2011]. This temperature offset is comparable to the difference between the bottom of the mixed layer and the base of the thermocline in modern surface waters off eastern New Zealand [*Garner*, 1961; *Heath*, 1975; *Locarnini et al*., 2006].

[39] Zn/Ca offsets between chambers *f-2* and *f* in core tops and plankton tows are also consistent with increasing Zn concentrations with water depth, following a nutrient-like distribution similar to Cd (Figure 3) [*Boyle*, 1981]. This indicates for the first time that the interchamber differences in *G. bulloides* Zn/Ca could be used to elucidate nutrient stratification in the upper water column. The down core Zn/Ca offset between chambers *f-2* and *f* shows a similar pattern to the Mg/Ca with reduced nutrient stratification in the glacial and no stratification/complete mixing of the upper water column during the ACR. Nutrient stratification appears to re-establish initially in the upper surface waters from circa 11.5 ka, prior to the stabilization of the mixed layer/thermocline after circa 10.5 ka [*Nelson et al*., 2000].

5.3. Glacial/Interglacial Changes in the SPG

[40] Changes in the wind fields across glacial-interglacial cycles probably affected the ancestral SPG, judging by the dependency of its modern counterpart on the wind stress curl [e.g., *Ridgway and Dunn*, 2007; *Tilburg et al*., 2001]. Here we evaluate the glacial/interglacial changes in the SPG from the presence of STW sourced from the gyre via the TF—the trans-Tasman component of the SPG (Figure 1). We combine the evidence from our new geochemical proxies, with previously published paleoceanographic data (Figure 8).

5.3.1. Glaciation

[41] During the glacial period, SAW dominated the MD97 2121 site as reflected by Mg/Ca *G. bulloides* temperatures, typically <11°C (Figures 4 and 8), and supported by a planktonic foraminiferal assemblage, which includes the polar species *Neogloboquadrina pachyderma* (Figure 5) [*Nelson et al*., 2000; *Weaver et al*., 1998]. The concomitant low Zn/Ca and Mn/Ca also support the presence of SAW north of the Chatham Rise (Figure 3). This is the result of a strengthened branch of the ACC, which forced SAW northward through Mernoo Saddle, thus circumventing the STF that is constrained by Chatham Rise (Figure 1) [*Sikes et al*., 2002; *Sutton and Roemmich*, 2001].

[42] Between 25 and 15 ka, Mg/Ca and Zn/Ca data from different chambers (chamber *f-2* minus *f*) of *G. bulloides* suggest reduced thermal (offset of <3°C) and nutrient stratification of the upper ocean (Figures 4 and 8). This coincides with a reduction in the offset between *G. bulloides* and *G. inflata* $\delta^{18}O$ data as well [*Carter et al*., 2008; Figure 4) and indicates that the upper water column was well mixed by the strong westerly winds during the glacial [*Shulmeister et al*., 2004]. The variance in the Mg/Ca, Zn/Ca, and Mn/Ca data from individual samples was also at its lowest during the glacial, suggesting that there may have been fewer or muted short-term fluctuations such as that caused by El Niño–Southern Oscillation (ENSO) activity (also modulated by the Southern Annular Mode) which affects storminess and ocean temperatures in the Hawke Bay region [*Gomez et al*., 2012]. However, this lower glacial Mg/Ca variance may also reflect a more limited calcification depth range for *G. bulloides*, owing to diminished upper ocean thermal stratification than during the interglacial period.

[43] Higher Mg/Ca SSTs at circa 22–18 ka, accompanied by elevated Zn/Ca, lightened planktic $\delta^{18}O$ and warmer water foraminiferal assemblages point to an incursion of STW that is also present at ODP 1123, downstream of MD97 2121 (Figures 4 and 7) [*Crundwell et al*., 2008]. No clear temperature change is recorded in Antarctica at this time period (Figure 4) [*Jouzel et al*., 2007], but there is a coeval warming in Greenland [*North Greenland Ice Core Project*, 2004]. We suggest that the perturbation may reflect Northern Hemispheric forcing of the equatorial region and midlatitude winds that spin-up the SPG under increased wind stress curl [cf. *Denton et al*., 2010; *Roemmich*, 2007].

5.3.2. Early Deglacial 17–14.5 ka - the "Mystery Interval"

[44] The Mystery Interval (MI)—a period of rapid and often contradictory change in the Northern Hemisphere [*Denton* et al., 2010]—coincides with rapid change in MD97 2121 (Figures 7 and 8). Millennial-scale MI events may be manifested in the Southern Hemisphere by the southward forcing of the Intertropical Convergence Zone [*Denton et al*., 2010]. In the Southern Hemisphere, the MI was accompanied by a poleward shift of zonal westerly winds, a general warming of the upper ocean [*Barrows et al*., 2007; *Calvo et al*., 2007], and increased Southern Ocean upwelling [*Anderson et al*., 2009].

[45] In contrast, *G. bulloides* Mg/Ca temperatures at MD97 2121decreased to the point that they converged on those of the subantarctic site MD97 2120 [*Pahnke et al*., 2003]. *G. bulloides* Zn/Ca and Mn/Ca levels increased slightly, and subpolar and polar planktic species reached a maximum (Figures 5 and 6). *G. bulloides* Mg/Ca decreases coupled with high-nutrient levels (Zn/Ca) and high $\delta^{13}C$ appear to confirm regional upwelling of cooler nutrient-rich water similar to, but on a much smaller scale than, that previously associated with diatom productivity blooms in the Southern Ocean [*Anderson et al*., 2009].

[46] However, the alkenone temperatures from MD97 2121 maintained a consistent increasing trend of approximately 0.4°C/ka [*Pahnke and Sachs*, 2006], similar to SSTs from the eastern equatorial Pacific Ocean [e.g., *Koutavas et al*., 2002; *Rosenthal et al*., 2003] and consistent with an incursion of STW resulting from a spin-up of the SPG. The decoupling of *G. bulloides* Mg/Ca from alkenone and later *G. ruber* temperatures may reflect changes in the species seasonality/ecological niches across this interval [*Leduc et al*., 2010; J. P. Marr et al., manuscript in preparation, 2013].

5.3.3. ACR to Late Deglaciation

[47] Large variability in foraminiferal Mg/Ca temperatures and Zn/Ca from 14 to 11.5 ka is representative of a dynamically mixed upper ocean with competing SAW and STW during the ACR (Figure 8). The ACR is bookended by peaks in *G. bulloides* and *G. ruber* abundance (Figure 6) as water masses over MD97 2121 shifted dominance from SAW to STW. Large swings in foraminifera SSTs of approximately 7°C are similar to other Southern Hemisphere cores which switch from SAW to STW [*Barrows et al*., 2007; *Calvo et al*., 2007; *Passlow et al*., 1997; *Sikes et al*., 2009]. These swings are accompanied here by marked changes in subsurface trace metal levels and an offset in planktic $\delta^{13}C$ (Figures 4 and 7). Thermal and nutrient surface water stratification during this time was also highly variable. There is a shift from moderate stratification during the early ACR, before stratification collapsed between circa 13.5–12.5 ka (Figure 4) [*Carter et al*., 2008]. This was followed by a decline in surface water productivity, before a gradual recovery and increase in thermal stratification by the late deglaciation (Figures 4 and 6). This condensed stratification during the ACR is likely the result of enhanced winds [*Carter et al*., 2008], either causing (i) increased physical mixing of the surface waters [*Carter et al*., 2008; *Shulmeister et al*., 2004] and/or (ii) regional upwelling along the nearby continental margin as seen in the modern ocean [e.g., *Heath*, 1972a; *Heath*, 1985].

[48] This intense ACR variability is representative of the competing equatorial-southern forcing; the latter driving SAW northward through the Mernoo Saddle during the last glaciation and ACR, and the former forcing STW southward during the late deglaciation/early Holocene.

5.3.4. Holocene

[49] At circa 11.5 ka, peak STW conditions were reached with thermal maxima from *G. ruber* Mg/Ca SST. The TF shifted south and likely found gaps in the Norfolk Ridge system that maximized the subtropical inflow to eastern New Zealand (Figure 8) [*Carter et al*., 2008]. Surface water thermal and nutrient stratification is strongest during the Holocene. Stratification is most prominent in the uppermost surface waters at 11.5 ka accompanied by a peak in biogenic siliceous and carbonate MAR/productivity (Figure 6). For the remainder of the Holocene, upper ocean temperature stratification was consistent, as shown by the offset between *G. bulloides* chambers *f-2* and *f* Mg/Ca ratios. However, isothermal conditions from 0 to approximately 75 m depth likely prevailed, as indicated by the similarity between *G. bulloides* chamber *f-2* and *G. ruber* Mg/Ca temperatures (Figure 4). Between 7 and 5.5 ka, *G. bulloides* Zn/Ca declines rapidly and merges with that of *G. ruber*. This convergence may represent a phase of reduced nutrient stratification in the mid-Holocene that is coeval with a period of high storm activity recorded in nearby onshore Lake Tutira [*Gomez et al*., 2012]. A 50% increase in the variance of the trace element/Ca data during the Holocene may suggest increased decadal or ENSO activity [*Koutavas et al*., 2002; *Koutavas et al*., 2006].

6. Conclusions

[50] In situ measurements on modern foraminifera from a wide range of environmental settings indicate that Zn/Ca, Mn/Ca, and Mg/Ca can act as proxies for the water masses and structure of the upper ocean. We show that Zn/Ca and Mn/Ca measurements in *G. bulloides* and *G. ruber* have the potential to trace SAW and STW surface water masses. Offsets between the Mg/Ca and Zn/Ca from chamber *f* and *f-2* data may also function as a proxy for thermal and nutrient stratification of the upper ocean.

[51] By applying these new proxies to down core data from MD97 2121, we show that the ocean off eastern New Zealand underwent significant changes over the past 25 kyr. At the Last Glacial Maximum, mean SSTs were approximately 6–7°C colder than those of the present, foraminiferal Mn/Ca and Zn/Ca were low, and ocean thermal and nutrient stratification was minimal. Such conditions reflect regional dominance of SAW under a strengthened ACC and a reduced STW inflow associated with a weakened SPG. SST perturbations from circa 22–18 ka were likely due to early deglacial

equatorial forcing that increased the STW inflow, raising Zn/Ca levels briefly. From 17.5 to 14.5 ka, an anomalous period occurred that coincides with the Northern Hemisphere "Mystery Interval." During this period, *G. bulloides* SSTs decreased by approximately 1°C/ka, while alkenone temperatures indicate continued surface ocean warming. Upper ocean thermal and nutrient stratification collapsed during the ACR when large swings in temperature and nutrient concentrations resulted from the interplay between polar-forced SAW and equatorial-derived STW. After the ACR, the continued poleward migration of strong zonal westerly winds strengthened the SPG and its STW inflow to eastern New Zealand. With this southward shift of strong winds, the upper ocean at core site MD97 2121 was dominated by generally well-stratified STW from circa 10 ka to the present.

[52] **Acknowledgments.** We thank Joel Baker from VUW for his role in instigating this project, technical assistance, and constructive comments that led to improvements in the manuscript. Monica Handler from VUW is also thanked for her constructive comments that led to improvements in the manuscript. Lisa Northcote and Helen Neil (NIWA) provided assemblage data and core top and down core samples. We thank Rob McKay, Gavin Dunbar, Andrew Mackintosh (VUW), and Martin Crundwell (GNS) for helpful discussions; Aidan Allan, Richard Tilley, and David Flynn from VUW for technical assistance; and Michael Ellwood from ANU for surface ocean trace element concentration data. The authors would also like to thank an anonymous reviewer and Chris Charles for their very helpful and constructive comments which have improved the manuscript.

References

Anand, P., H. Elderfield, and M. H. Conte (2003), Calibration of Mg/Ca thermometry in planktonic foraminifera from a sediment trap time series, *Paleoceanography*, *18*(2), 1050, doi:10.1029/2002PA000846.

Anderson, R. F., S. Ali, L. I. Bradtmiller, S. H. H. Nielsen, M. Q. Fleisher, B. E. Anderson, and L. H. Burckle (2009), Wind-driven upwelling in the Southern Ocean and the deglacial rise in atmospheric CO_2, *Science*, *323*(5920), 1443–1448.

Barrows, T. T., S. Juggins, P. De Deckker, E. Calvo, and C. Pelejero (2007), Long-term sea surface temperature and climate change in the Australian-New Zealand region, *Paleoceanography*, *22*, PA2215, doi:10.1029/2006PA001328.

Berger, W. H. (1971), Sedimentation of planktonic foraminifera, *Mar. Geol.*, *11*(5), 325–358.

Boiteau, R., M. Greaves, and H. Elderfield (2012), Authigenic uranium in foraminiferal coatings: A proxy for ocean redox chemistry, *Paleoceanography*, *27*, PA3227, doi:10.1029/2012PA002335.

Bolton, A., and J. P. Marr (2013), Trace element variability in crust-bearing and non crust-bearing *Neogloboquadrina incompta*, P-D intergrade and *Globoconella inflata* from the Southwest Pacific Ocean: Potential paleoceanographic implications, *Mar. Micropaleontol.*, 100, 21–33.

Bolton, A., J. A. Baker, G. B. Dunbar, L. Carter, E. G. C. Smith, and H. L. Neil (2011), Environmental versus biological controls on Mg/Ca variability in *Globigerinoides ruber* (white) from core top and plankton tow samples in the southwest Pacific Ocean, *Paleoceanography*, *26*, PA2219, doi:10.1029/2010PA001924.

Bostock, H. C., B. W. Hayward, H. L. Neil, K. I. Currie, and G. B. Dunbar (2011), Deep-water carbonate concentrations in the southwest Pacific, *Deep Sea Res. Part I*, *58*(1), 72–85.

Bowie, A. R., D. Lannuzel, T. A. Remenyi, T. Wagener, P. J. Lam, P. W. Boyd, C. Guieu, A. T. Townsend, and T. W. Trull (2009), Biogeochemical iron budgets of the Southern Ocean south of Australia: Decoupling of iron and nutrient cycles in the subantarctic zone by the summertime supply, *Global Biogeochem. Cycles*, *23*, GB4034, doi:10.1029/2009GB003500.

Boyd, P., J. LaRoche, M. Gall, R. Frew, and R. M. L. McKay (1999), Role of iron, light, and silicate in controlling algal biomass in subantarctic waters SE of New Zealand, *J. Geophys. Res.*, *104*(C6), 13,395–13,408.

Boyle, E. A. (1981), Cadmium, zinc, copper, and barium in foraminifera tests, *Earth Planet. Sci. Lett.*, *53*(1), 11–35.

Boyle, E. A. (1983), Manganese carbonate overgrowths on foraminifera tests, *Geochim. Cosmochim. Acta*, *47*(10), 1815–1819.

Brown, S. J., and H. Elderfield (1996), Variations in Mg/Ca and Sr/Ca ratios of planktonic foraminifera caused by postdepositional dissolution: Evidence of shallow Mg-dependent dissolution, *Paleoceanography*, *11*(5), 543–551.

Bruland, K. W., and M. C. Lohan (2003), 6.02—Controls of trace metals in seawater, in *Treatise on Geochemistry*, edited by D. H. Heinrich, and K. T. Karl, pp. 23–47, Pergamon, Oxford, U. K.

Calvo, E., C. Pelejero, P. De Deckker, and G. A. Logan (2007), Antarctic deglacial pattern in a 30 kyr record of sea surface temperature offshore South Australia, *Geophys. Res. Lett.*, *34*, L13707, doi:10.1029/2007GL029937.

Carter, L., and B. Manighetti (2006), Glacial/interglacial control of terrigenous and biogenic fluxes in the deep ocean off a high input, collisional margin: A 139 kyr record from New Zealand, *Mar. Geol.*, *226*(3–4), 307–322.

Carter, L., B. Manighetti, G. Ganssen, and L. Northcote (2008), Southwest Pacific modulation of abrupt climate change during the Antarctic Cold Reversal-Younger Dryas, *Palaeogeogr. Palaeoclimatol. Palaeoecol.*, *260*(1–2), 284–298.

Chiswell, S. M. (2002), Temperature and salinity mean and variability within the subtropical front over the Chatham Rise, New Zealand, *N. Z. J. Mar. Freshwater. Res.*, *36*(2), 281–298.

Chiswell, S. M. (2005), Mean and variability in the Wairarapa and Hikurangi Eddies, New Zealand, *N. Z. J. Mar. Freshwater Res.*, *39*, 121–134.

Cléroux, C., E. Cortijo, P. Anand, L. Labeyrie, F. Bassinot, N. Caillon, and J.-C. Duplessy (2008), Mg/Ca and Sr/Ca ratios in planktonic foraminifera: Proxies for upper water column temperature reconstruction, *Paleoceanography*, *23*, PA3214, doi:10.1029/2007PA001505.

Croot, P. L., and K. A. Hunter (1998), Trace metal distributions across the continental shelf near Otago Peninsula, New Zealand, *Mar. Chem.*, *62*(3–4), 185–201.

Crundwell, M., G. H. Scott, T. R. Naish, and L. Carter (2008), Glacial-interglacial ocean climate variability from planktonic foraminifera during the Mid-Pleistocene transition in the temperate Southwest Pacific, ODP Site 1123, *Palaeogeogr. Palaeoclimatol. Palaeoecol.*, *260*(1–2), 202–229.

Denton, G. H., R. F. Anderson, J. R. Toggweiler, R. L. Edwards, J. M. Schaefer, and A. E. Putnam (2010), The last glacial termination, *Science*, *328*(5986), 1652–1656.

Dixon, W. J., and F. J. Massey (1969), *Introduction to Statistical Analysis*, 3rd ed., McGraw-Hill, Tokyo.

Eggins, S., P. De Deckker, and J. Marshall (2003), Mg/Ca variation in planktonic foraminifera tests: Implications for reconstructing palaeo-seawater temperature and habitat migration, *Earth Planet. Sci. Lett.*, *212*(3–4), 291–306.

Eggins, S. M., A. Sadekov, and P. De Deckker (2004), Modulation and daily banding of Mg/Ca in *Orbulina universa* tests by symbiont photosynthesis and respiration: A complication for seawater thermometry?, *Earth Planet. Sci. Lett.*, *225*(3–4), 411–419.

Ellwood, M. J., P. W. Boyd, and P. Sutton (2008), Winter-time dissolved iron and nutrient distributions in the Subantarctic Zone from 40–52S; 155–160E, *Geophys. Res. Lett.*, *35*, L11604, doi:10.1029/2008GL033699.

European Project for Ice Coring in Antarctica (2004), Eight glacial cycles from an Antarctic ice core, *Nature*, *429*(6992), 623–628.

Gaillardet, J., J. Viers, and B. Dupré (2003), Trace elements in river waters, in *Treatise on Geochemistry*, edited by D. H. Heinrich and K. T. Karl, pp. 225–272, Pergamon, Oxford, U. K.

Garner, D. M. (1961), *Hydrology of New Zealand Coastal Waters, 1955*, N. Z. Oceanogr. Inst., Wellington.

Gomez, B., L. Carter, A. R. Orpin, K. M. Cobb, M. J. Page, N. A. Trustrum, and A. S. Palmer (2012), ENSO/SAM interactions during the middle and late Holocene, *Holocene*, *22*(1), 23–30.

Hall, J. M., and L. H. Chan (2004), Ba/Ca in *Neogloboquadrina pachyderma* as an indicator of deglacial meltwater discharge into the western Arctic Ocean, *Paleoceanography*, *19*, PA1017, doi:10.1029/2003PA000910.

Heath, R. A. (1972a), Choice of a reference surface for geostrophic currents around New Zealand, *New Zealand Journal of Marine and Freshwater Research*, *6*, 148–177.

Heath, R. A. (1972b), Oceanic upwelling produced by northerly winds on the north Canterbury coast, New Zealand, *New Zealand Journal of Marine and Freshwater Research*, *6*, 348–351.

Heath, R. A. (1975), *Oceanic Circulation and Hydrology off the Southern Half of South Island, New Zealand*, 36 pp., N. Z. Oceanogr. Inst., Wellington.

Heath, R. (1985), A review of the physical oceanography of the seas around New Zealand—1982, *N. Z. J. Mar. Freshwater Res.*, *19*(79), 79–124.

Hedenquist, J. W., S. F. Simmons, W. F. Giggenbach, and C. S. Eldridge (1993), White Island, New Zealand, volcanic-hydrothermal system represents the geochemical environment of high-sulfidation Cu and Au ore deposition, *Geology*, *21*(8), 731–734.

Hemleben, C., M. Spindler, and O. R. Anderson (1989), *Modern Planktonic Foraminifera*, Springer-Verlag, New York.

Hicks, D. M., and U. Shankar (2003), *Sediment From New Zealand Rivers*, p. 236, Natl. Inst. of Water and Atmos. Res., Wellington.

Ho, T.-Y., A. Quigg, Z. V. Finkel, A. J. Milligan, K. Wyman, P. G. Falkowski, and F. M. M. Morel (2003), The elemental composition of some marine phytoplankton, *J. Phycol.*, *39*(6), 1145–1159.

Hönisch, B., K. A. Allen, A. D. Russell, S. M. Eggins, J. Bijma, H. J. Spero, D. W. Lea, and J. Yu (2011), Planktic foraminifers as recorders of seawater Ba/Ca, *Mar. Micropaleontol.*, *79*(1–2), 52–57.

Imbrie, J., and N. G. Kipp (1971), A new micropaleontological method for quantitative paleoclimatology: application to a late Pleistocene Caribbean core, in *The Late Cenozoic Glacial Ages*, edited by K. K. Turekian, pp. 71–181, Yale Univ. Press, New Haven, Conn.

Jacquet, S. H. M., F. Dehairs, and S. Rintoul (2004), A high resolution transect of dissolved barium in the Southern Ocean, *Geophys. Res. Lett.*, *31*, L14301, doi:10.1029/2004GL020016.

Jouzel, J., et al. (2007), Orbital and millennial Antarctic climate variability over the past 800,000 years, *Science*, *317*(5839), 793–796.

Klinkhammer, G. P., and M. L. Bender (1980), The distribution of manganese in the Pacific Ocean, *Earth Planet. Sci. Lett.*, *46*(3), 361–384.

Koutavas, A., J. Lynch-Stieglitz, T. M. Marchitto, and J. P. Sachs (2002), El Niño-like pattern in ice age tropical Pacific sea surface temperature, *Science*, *297*(5579), 226–230.

Koutavas, A., P. B. deMenocal, G. C. Olive, and J. Lynch-Stieglitz (2006), Mid-Holocene El Niño–Southern Oscillation (ENSO) attenuation revealed by individual foraminifera in eastern tropical Pacific sediments, *Geology*, *34*(12), 993–996.

Lea, D. W., and E. A. Boyle (1990), Foraminiferal reconstruction of barium distributions in water masses of the glacial oceans, *Paleoceanography*, *5*(5), 719–742.

Lea, D. W., and E. A. Boyle (1991), Barium in planktonic foraminifera, *Geochim. Cosmochim. Acta*, *55*(11), 3321–3331.

Lea, D. W., and H. J. Spero (1994), Assessing the reliability of paleochemical tracers: Barium uptake in the shells of planktonic foraminifera, *Paleoceanography*, *9*(3), 445–452.

Leduc, G., R. Schneider, J. H. Kim, and G. Lohmann (2010), Holocene and Eemian sea surface temperature trends as revealed by alkenone and Mg/Ca paleothermometry, *Quat. Sci. Rev.*, *29*(7–8), 989–1004.

Locarnini, R. A., A. V. Mishonov, J. I. Antonov, T. P. Boyer, and H. E. Garcia (2006), Hydrographic data, in *World Ocean Atlas 2005*, NOAA Atlas NESDIS, vol. 61, edited by S. Levitus, pp. 182, Gov. Print. Off., Washington, D.C.

Lorrey, A. M., et al. (2012), Palaeocirculation across New Zealand during the Last Glacial Maximum at ~21 ka, *Quat. Sci. Rev.*, *36*, 189–213.

Marchitto, T. M., Jr., W. B. Curry, and D. W. Oppo (2000), Zinc concentrations in benthic foraminifera reflect seawater chemistry, *Paleoceanography*, *15*(3), 299–306.

Marr, J. P., J. A. Baker, L. Carter, A. S. R. Allan, G. B. Dunbar, and H. C. Bostock (2011), Ecological and temperature controls on Mg/Ca ratios of *Globigerina bulloides* from the southwest Pacific Ocean, *Paleoceanography*, *26*, PA2209, doi:10.1029/2010PA002059.

Marr, J. P., H. C. Bostock, L. Carter, A. Bolton, and E. Smith (2013), Differential effects of contrasting cleaning procedures on the trace element chemistry of planktic foraminifera, *Chem. Geol.*. doi:10.1016/j.chemgeo.2013.05.019, in press.

Martin, J. H., R. M. Gordon, S. Fitzwater, and W. W. Broenkow (1989), Vertex: Phytoplankton/iron studies in the Gulf of Alaska, *Deep Sea Res. Part A*, *36*(5), 649–680.

Morel, F. M. M., and N. M. Price (2003), The biogeochemical cycles of trace metals in the oceans, *Science*, *300*(5621), 944–947.

Morel, F. M. M., A. J. Milligan, and M. A. Saito (2003), Marine bioinorganic chemistry: The role of trace metals in the oceanic cycles of major nutrients, in *Treatise on Geochemistry*, edited by D. H. Heinrich and K. T. Karl, pp. 113–143, Pergamon, Oxford, U. K.

Morris, M., B. Stanton, and H. Neil (2001), Subantarctic oceanography around New Zealand: Preliminary results from an ongoing survey, *N. Z. J. Mar. Freshwater Res.*, *35*(3), 499–519.

Nelson, C. S., I. L. Hendy, H. L. Neil, C. H. Hendy, and P. P. E. Weaver (2000), Last glacial jetting of cold waters through the Subtropical Convergence zone in the Southwest Pacific off eastern New Zealand, and some geological implications, *Palaeogeogr. Palaeoclimatol. Palaeoecol.*, *156*(1–2), 103–121.

North Greenland Ice Core Project (2004), High-resolution record of Northern Hemisphere climate extending into the last interglacial period, *Nature*, *431*(7005), 147–151.

Northcote, L., H. Neil, and B. Manighetti (2007), *Global Change Through Time, Objective 1, Quaternary Climate and Biota-Foraminiferal Census*, Natl. Inst. of Water and Atmos. Res., Wellington.

Pahnke, K., and J. P. Sachs (2006), Sea surface temperatures of southern midlatitudes 0–160 kyr BP, *Paleoceanography*, *21*, PA2003, doi:10.1029/2005PA001191.

Pahnke, K., R. Zahn, H. Elderfield, and M. Schulz (2003), 340,000-year centennial-scale marine record of Southern Hemisphere climatic oscillation, *Science*, *301*(5635), 948–952.

Passlow, V., W. Pinxian, and A. R. Chivas (1997), Late Quaternary palaeoceanography near Tasmania, southern Australia, *Palaeogeogr. Palaeoclimatol. Palaeoecol.*, *131*(3–4), 433–463.

Pearce, N., W. Perkins, J. Westgate, M. Gorton, S. Jackson, C. Neal, and S. Cheney (1997), New data for National Institute of Standards and Technology 610 and 612 glass reference materials, *Geostand. Newsl.*, *21*, 115–144.

Price, N. M., and F. M. M. Morel (1990), Cadmium and cobalt substitution for zinc in a marine diatom, *Nature*, *344*(6267), 658–660.

Ridgway, K. R., and J. R. Dunn (2007), Observational evidence for a Southern Hemisphere oceanic supergyre, *Geophys. Res. Lett.*, *34*, L13612, doi:10.1029/2007GL030392.

Ridgway, K. R., and K. Hill (2009), The East Australian Current, in *A Marine Climate Change Impacts and Adaptation Report Card for Australia 2009*, edited by E.S. Poloczanska, A.J. Hobday, and A.J. Richardson, Natl. Clim. Change Adapt. Res. Fac., Cleveland, Ohio.

Roemmich, D. (2007), Physical oceanography: Super spin in the southern seas, *Nature*, *449*(7158), 34–35.

Roemmich, D., and P. Sutton (1998), The mean and variability of ocean circulation past northern New Zealand: Determining the representativeness of hydrographic climatologies, *J. Geophys. Res.*, *103*(C6), 13,041–13,054.

Rosenthal, Y., M. P. Field, and R. M. Sherrell (1999), Precise determination of element/calcium ratios in calcareous samples using sector field inductively coupled plasma mass spectrometry, *Anal. Chem.*, *71*(15), 3248–3253.

Rosenthal, Y., D. W. Oppo, and B. K. Linsley (2003), The amplitude and phasing of climate change during the last deglaciation in the Sulu Sea, western equatorial Pacific, *Geophys. Res. Lett.*, *30*(8), 1428, doi:10.1029/2002GL016612.

Sadekov, A. Y., S. M. Eggins, and P. De Deckker (2005), Characterization of Mg/Ca distributions in planktonic foraminifera species by electron microprobe mapping, *Geochem. Geophys. Geosyst.*, *6*, Q12P06, doi:10.1029/2005GC000973.

Sadekov, A., S. M. Eggins, P. De Deckker, and D. Kroon (2008), Uncertainties in seawater thermometry deriving from intratest and intertest Mg/Ca variability in *Globigerinoides ruber*, *Paleoceanography*, *23*, PA1215, doi:10.1029/2007PA001452.

Shulmeister, J., et al. (2004), The Southern Hemisphere westerlies in the Australasian sector over the last glacial cycle: A synthesis, *Quat. Int.*, *118–119*(0), 23–53.

Sikes, E. L., W. R. Howard, H. L. Neil, and J. K. Volkman (2002), Glacial-interglacial sea surface temperature changes across the subtropical front east of New Zealand based on alkenone unsaturation ratios and foraminiferal assemblages, *Paleoceanography*, *17*(2), 1012, doi:10.1029/2001PA000640.

Sikes, E. L., W. R. Howard, C. R. Samson, T. S. Mahan, L. G. Robertson, and J. K. Volkman (2009), Southern Ocean seasonal temperature and Subtropical Front movement on the South Tasman Rise in the late Quaternary, *Paleoceanography*, *24*, PA2201, doi:10.1029/2008PA001659.

Spero, H. J., S. Eggins, A. Russell, L. Vetter, and B. Hoenisch (2008), Experimental perspective on cause of planktonic foraminifera intrashell Mg/Ca variability and impact on paleoceanographic applications, *Eos Trans. AGU*, *89*(53), Fall Meet. Suppl., Abstract PP41F-01.

Stuiver, M., T. F. Braziunas, P. M. Grootes, and G. A. Zielinski (1997), Is there evidence for solar forcing of climate in the GISP2 oxygen isotope record?, *Quat. Res.*, *48*(3), 259–266.

Sutton, P. J. H. (2003), The Southland Current: A subantarctic current, *N. Z. J. Mar. Freshwater Res.*, *37*(3), 645–652.

Sutton, P., and D. Roemmich (2001), Ocean temperature climate off north-east New Zealand, *N. Z. J. Mar. Freshwater Res.*, *35*(3), 553–566.

Tilburg, C. E., H. E. Hurlburt, J. J. O'Brien, and J. F. Shriver (2001), The dynamics of the East Australian Current system: The Tasman Front, the East Auckland Current, and the East Cape Current, *J. Phys. Oceanogr.*, *31*(10), 2917–2943.

Weaver, P. P. E., H. Neil, and L. Carter (1997), Sea surface temperature estimates from the Southwest Pacific based on planktonic foraminifera and oxygen isotopes, *Palaeogeogr. Palaeoclimatol. Palaeoecol.*, *131*(3–4), 241–256.

Weaver, P. P. E., L. Carter, and H. L. Neil (1998), Response of surface water masses and circulation to late Quaternary climate change east of New Zealand, *Paleoceanography*, *13*(1), 70–83.

Webster, J. G. (1995), Chemical processes affecting trace metal transport in the Waihou River and estuary, New Zealand, *N. Z. J. Mar. Freshwater Res.*, *29*(4), 539–553.

Weldeab, S., D. W. Lea, R. R. Schneider, and N. Andersen (2007), 155,000 years of West African Monsoon and ocean thermal evolution, *Science*, *316*(5829), 1303–1307.